

Quantifying contributions of natural and anthropogenic dust emission from different climatic regions

Siyu Chen^a, Nanxuan Jiang^a, Jianping Huang^{a,*}, Xiaoguang Xu^b, Huiwei Zhang^a, Zhou Zang^a, Kangning Huang^c, Xiaocong Xu^d, Yun Wei^a, Xiaodan Guan^a, Xiaorui Zhang^a, Yuan Luo^a, Zhiyuan Hu^a, Taichen Feng^a

^a Key Laboratory for Semi-Arid Climate Change of the Ministry of Education, Lanzhou University, Lanzhou, 730000, China

^b Department of Chemical and Biochemical Engineering, The University of Iowa, Iowa City, IA, 42242, United States

^c Yale School of Forestry and Environmental Studies, Yale University, New Haven, CT 06511, United States

^d School of Geography and Planning, Guangdong Key Laboratory for Urbanization and Geo-simulation, Sun Yat-sen University, Guangzhou, 510275, China

ARTICLE INFO

Keywords:

Natural dust emissions
Anthropogenic dust emissions
Dynamic dust sources
Climatic regions

ABSTRACT

To quantitatively estimate the divergences in the natural and anthropogenic dust emission fluxes among different climatic regions, the total dust emissions at the global scale from 2007 to 2010 were simulated in this study. Despite the widely scattered anthropogenic dust distribution, the total area of potential anthropogenic dust sources was found slightly higher than that of natural dust sources. The anthropogenic dust distribution area was $1.61 \times 10^7 \text{ km}^2$ in January and $1.54 \times 10^7 \text{ km}^2$ in July, respectively. The natural dust sources contributed 81.0% of the global dust emissions and the anthropogenic contributed 19.0% of the residual. The natural and anthropogenic dust emission flux was $6.34 \pm 0.31 \mu\text{g m}^{-2} \text{ s}^{-1}$ and $1.01 \pm 0.07 \mu\text{g m}^{-2} \text{ s}^{-1}$, respectively. Especially, natural and anthropogenic dust emissions situated in different climatic regions. Natural dust emissions mainly located in hyper-arid and arid regions such as the Sahara, Arabian and Taklimakan Desert where dust emission fluxes range from 1 to $50 \mu\text{g m}^{-2} \text{ s}^{-1}$, accounted for 97.3% of natural dust emissions at the global scale. While anthropogenic dust emissions concentrate in semi-arid, sub-humid and humid regions and generally fluctuated between 0.1 and $10 \mu\text{g m}^{-2} \text{ s}^{-1}$. In addition, natural and anthropogenic dust proportions in semi-arid regions were the most complicated due to the complex land cover types, including grasslands, urban areas, croplands and open shrub lands, resulting in 42.99% of the anthropogenic dust emissions in semi-arid regions. The complex interplay of natural and anthropogenic dust emissions contributing to the total dust loadings may be a crucial factor enhanced the warming over semi-arid regions. This study provided confidence for the further investigation of the climatic impacts of natural and anthropogenic dust in different climatic regions under the background of global warming, especially the strengthening warming in semi-arid regions.

1. Introduction

Dust emission serves as a crucial part of the dust cycle, which further determines long-range dust transport and dust deposition processes as well as climate changes induced by dust (Qian et al., 1999; Gong et al., 2003, 2004, 2006; Shao et al., Mao et al., 2011, 2011; Zhao et al., 2010, 2013; Zhao et al., 2012; Liu et al., 2016; Chen et al., 2017a). Dust aerosols are divided into natural dust and anthropogenic dust according to their different dust source regions (Tegen and Fung, 1995; Tegen et al., 2004; Ginoux et al., 2001, 2012). Natural dust emissions mainly originate from bare surfaces such as deserts and Gobi Desert (Shao, 2004, 2011; Zhao et al., 2013; Chen et al., 2013, 2014a; 2017a).

Increasing efforts have been constantly devoted to improve natural dust emission schemes under various simplifications and hypotheses since the 1990s (Westphal et al., 1988; Jousaume, 1990; Tegen and Fung, 1994; Shao et al., 1996; Marticorena et al., 1997; Wang et al., 2000; Woodward, 2001; Zender et al., 2003; Sugimoto et al., 2003; Han et al., 2004, 2010; Wang et al., 2000, 2000; Huneus et al., 2010). Specifically, Shao and Dong (2006) divided dust emission schemes into three categories: (1) the empirical dust emission scheme such as those of Tegen and Fung (1995), Mahowald et al. (1999) and Perlwitz et al. (2001); (2) the dust emission scheme with simplified physical processes as used by Ginoux et al. (2001) and Woodward (2001); and (3) the detailed micro-physical dust emission scheme such as those of

* Corresponding author.

E-mail address: hjp@lzu.edu.cn (J. Huang).

<https://doi.org/10.1016/j.atmosenv.2018.07.043>

Received 10 April 2018; Received in revised form 20 July 2018; Accepted 25 July 2018

Available online 04 August 2018

1352-2310/© 2018 The Authors. Published by Elsevier Ltd. This is an open access article under the CC BY license (<http://creativecommons.org/licenses/by/4.0/>).

Marticorena and Bergametti (1995) and Shao (1996, 2001, 2004).

However, more and more researchers have noted that human activity can also induce dust emissions at the global scale (Penner et al., 1994; Tegen and Fung, 1995; Ginoux et al., 2012; Huang et al., 2015). Anthropogenic dust emissions can be interpreted as soil particles that originate from soil conditions being altered or disrupted by human activity (Tegen and Fung, 1995; Shao, 2004; Zender et al., 2004; Xi and Sokolik, 2016; Zheng et al., 2016; Chen et al., 2017b; Luan et al., 2017). Studies showed that the contribution of anthropogenic dust emissions was non-negligible to dust concentrations at the global scales (Huang et al., 2015; Guan et al., 2016; Chen et al., 2017c; Zhao et al., 2018). In previous studies related to dust emission models, only natural dust emissions were considered, while anthropogenic dust emissions induced by human activity were commonly ignored. Anthropogenic dust emission can be categorized into direct and indirect anthropogenic dust emissions based on different anthropogenic dust emission mechanisms. Different dust emission schemes were developed to simulate indirect and direct anthropogenic dust emissions, which can effectively capture the spatio-temporal distributions of anthropogenic dust emissions consistent with the anthropogenic dust column determined from CALIPSO retrievals.

The surface air temperature shows an overall warming and the large regional warming differences under the background of global warming (Huang et al., 2012, 2017a,b; Guan et al., 2015; Shukla and Mintz, 1982; Wu et al., 2011; Wallace and Johanson, 2012). Warming over land is significantly exceeding the global mean surface warming due to the lower warming over oceans (Dai, 2016). Huang et al. (2012, 2017a,b) noted that the enhanced warming in drylands has been 20–40% higher than that over humid lands. The climatic impacts of absorbing aerosols are highly concentrated because they can strongly absorb solar radiation and have a profound impact on climate change at the global and regional scale (Tegen and Fung, 1995; Foster and Rideout, 2007; Han et al., 2004, 2010; Shao et al., 2011; Chen et al., 2013, 2014a, b; Zhao et al., 2014; Kang et al., 2015, 2017). Kang et al. (2017) noted that different kinds of absorbing aerosols play its role in climate change over different climatic regions based on the Ozone Monitoring Instrument (OMI) satellite retrievals.

Dust aerosol, as an absorbing aerosol, strongly absorbs radiation and heats the atmosphere, playing an essential part in the hydrologic cycle, the carbon cycle, and the energy budget of the Earth system (Tegen and Fung, 1995; Foster and Rideout, 2007; Han et al., 2004, 2010; Shao et al., 2011; Chen et al., 2013, 2014a, b; Zhao et al., 2014; Kang et al., 2015, 2017). What are the characteristics of natural and anthropogenic dust emissions in different climatic regions? How much do anthropogenic and natural dust emissions contribute in different land cover types? The differences of the spatio-temporal distributions between natural and anthropogenic dust emissions were investigated in the study. The contributions of natural and anthropogenic dust emissions from different climatic regions were further compared and discussed.

2. Method and datasets

2.1. Datasets

2.1.1. Land cover datasets

The Collection 5.1 MODIS global land cover type climate modeling grid product (MCD12C1) from 2010 was utilized to identify the potential natural and indirect anthropogenic dust sources. This product has a 0.05° spatial resolution with 17 land cover types covered by different vegetation. The surface vegetation types were derived from the International Geosphere-Biosphere Programme (IGBP) (Friedl et al., 2010), which provided the dominant land cover types as well as the sub-grid frequency distribution of the land cover classes within 0.05° grid cells. Open shrub lands, savannas and barren or sparsely vegetated areas were selected as potential natural dust sources. Grasslands,

croplands and cropland mosaics were chosen as potential indirect anthropogenic dust sources, which is consistent with Huang et al. (2015) and Guan et al. (2016). A cropland mosaic is an area where the mosaic of croplands covers less than 60% of the landscape (Friedl et al., 2002). To reflect the changes in the surface conditions of potential dust source regions among the different seasons, NDVI derived from the Advanced Very High Resolution Radiometer (AVHRR) with a spatial resolution of 8 km and a two-week temporal resolution was used to investigate the seasonal variations in the surface bareness.

2.1.2. ERA-interim

ERA-Interim is a popular global atmospheric reanalysis product provided by the European Center for Medium-Range Weather Forecasts (ECMWF). It covers the period from 1 January 1979 to near-real time (Dee et al., 2011). Its wind speed datasets at 10 m with a 6-h interval and a 0.4° × 0.4° spatial resolution were utilized in this study to calculate natural and indirect anthropogenic dust emissions. As illustrated in Largeron et al. (2015), the ERA-Interim wind speed at 10 m well captures the spatio-temporal distribution of the dust emission derived from wind erosion compared with NCEP-CFSR and MERRA reanalysis products. The annual biases of wind speed from the ERA-Interim, NCEP-CFSR and MERRA products are 0.27 m s⁻¹, -0.62 m s⁻¹ and 0.70 m s⁻¹ compared with wind speed data from observations, respectively. Marsham et al. (2011) indicated that the calculated dust emission fluxes using the wind speed at 10 m from ERA-Interim are capable of capturing the spatio-temporal distributions of both indirect anthropogenic and natural dust emissions.

2.1.3. Aridity index (AI)

The aridity index (AI) is defined as the ratio of annual precipitation to annual potential evapotranspiration, which represents the evaporation demand of the atmosphere. The AI indicates the degree of water deficiency and can effectively reflect the level of climatic dryness (Feng and Fu, 2013). In this study, observational data from the Climate Prediction Center (CPC) were used to calculate the AI, so as to classify the different types of climatic regions. Under this quantitative indicator, drylands are commonly defined as regions with an AI < 0.5, and the world can be further subdivided into five climate parts: hyper-arid (AI < 0.05), arid (0.05 < AI < 0.2), semi-arid (0.2 < AI < 0.5), sub-humid (0.5 ≤ AI < 0.65) and humid (AI sub-humid (0.5 ≤ AI < 0.65) and humid (AI sub-humid (0.5 ≤ AI < 0.2), semiUn Hulme, 1996; Huang et al., 2012). It is obvious that drier regions have smaller AI values. The AI datasets were provided by Feng and Fu (2013) with a spatial resolution of 0.5° × 0.5° and a temporal coverage from 1948 to 2008.

2.1.4. Night light datasets

Nighttime light (NTL) datasets obtained by the DMSP/OLS sensors are commonly employed to extract the spatial distributions of urbanization (Elvidge et al., 1997). However, as illustrated in Zhang et al. (2013, 2016), NTL data are limited by the saturation of data values, especially in urban cores, and by the inconsistencies in their temporal signals. Therefore, a consistent NTL time series together with a new spectral index which was named as the vegetation adjusted NTL urban index (VANUI) constructed based on the NTL data were used to replace the NTL data to calculate the CNLI (compounded night light index) in this study. As urban areas are the dominant contributors to direct anthropogenic dust emissions, CNLI, the index indicating the urbanization level with a range from 0 to 1, was employed to identify potential direct anthropogenic dust sources. More details for the calculation of the CNLI can be found in Zhuo et al. (2003).

2.1.5. Population density

The population density data was derived from version3 of the gridded population of the world dataset (GPWv3), which is favored by the Center for International Earth Science Information Network (CIESIN) and the Centro Internacional de Agricultura Tropical (CIAT)

(<http://sedac.ciesin.columbia.edu/data/collection/gpw-v3>). The $0.5^\circ \times 0.5^\circ$ spatial resolution and five-year temporal resolution from 1990 to 2010 of the population data effectively describe the global population distribution. In this study, these population data in 2010 was used to quantify the intensities of human activities.

2.1.6. Gross domestic product (GDP)

The gross domestic product (GDP) at the global scale was down-scaled at $0.5^\circ \times 0.5^\circ$ resolution from 1980 to 2100 by Murakami and Yamagata (2017), considering the spatial and economic interaction among cities and multiplying auxiliary variables accurately. The actual GDPs from 1980 to 2010 and estimated GDPs under different Shared Socioeconomic Pathways (SSPs) were provided from 2010 to 2100. In this study, the actual GDPs in 2010 and 2000 were utilized to obtain the GDP growth at the global scale. This dataset is available at <http://www.cger.nies.go.jp/gcp/population-and-gdp.html>.

2.1.7. MISR dust aerosol optical depth

MISR is a scientific multi-angle imaging spectroradiometer instrument onboard Terra satellite launched on 18 December 1999 by NASA (Kahn et al., 1998, 2001). The dust aerosol optical depth (DOD) retrieved from MISR has been employed to compare dust emission simulations results with observations (Zhang and Christopher, 2003; Kim et al., 2013; Kalashnikova and Kahn, 2008; Wang et al., 2012), showing great capacities in capturing the characteristics of dust aerosol. Therefore, in this study, the dust AOD originated from MISR was utilized to ensure the feasibility of our simulations at the global scale.

2.1.8. Soil moisture

The soil moisture datasets were utilized in this study to investigate the influencing factor towards the direct anthropogenic dust emissions. The datasets were derived from the Noah 2.7.1 model in the Global Land Data Assimilation Systems (GLDAS) whose simulation was forced by the combination of NOAA/GDAS atmospheric analysis field disaggregated by NOAA Climate Prediction Center Merged Analysis of Precipitation (CMAP) fields. The temporal and spatial resolution of the soil moisture were monthly and $1^\circ \times 1^\circ$ respectively.

2.2. Method

2.2.1. Dynamic dust source regions

Previous studies always employed static land cover types to classify potential dust sources, introducing great uncertainties in estimating dust emissions in different seasons (Kim et al., 2013, 2017; Mao et al., 2013). Therefore, a dynamic bareness map with a $1^\circ \times 1^\circ$ resolution was constructed by employing the 8 km-resolution NDVI data (Kim et al., 2013). The corresponding formula is as follows:

$$B = \frac{N_{<0.15}}{N_{total}} \quad (1)$$

where $N_{<0.15}$ and N_{total} are the number of NDVI pixels below a value of 0.15 (Tucker et al., 1991; Peters and Eve, 1995; Sobrino and Raissouni, 2000; Bradley and Mustard, 2005) and the total number of NDVI pixels within a $1^\circ \times 1^\circ$ grid cell, respectively (Brown et al., 2006).

2.2.2. Natural dust emission scheme

The widely known dust emission scheme introduced by Marticorena and Bergametti (1995) (hereinafter referred to as MB) provides the vertical dust mass flux in bare-soil surface. The MB scheme contains various affecting factors that are hard to obtain precisely, resulting in difficulties of the simulations utilized in this dust emission scheme. To isolate land surface features and their meteorological impacts, Marsham et al. (2011) only retained the wind-related terms in the MB scheme by employing wind speed at 10 m (u) to replace the friction velocity (u_*), and their simulation results were consistent with the result of Cakmur et al. (2004). In addition, Evan et al. (2016) employed the formula from

Marsham et al. (2011) to simulate African dust uplifting and their results reproduced dust emissions in North Africa very well. Therefore, a simplified formula can be used to define the natural dust emission flux as follows:

$$G_{natural} = C \times B \times u^3 \times \left(1 + \frac{u_t}{u}\right) \times \left(1 - \frac{u_t^2}{u^2}\right), \text{ if } u > u_t \quad (2)$$

where C is an empirical constant, B is the dynamic surface bareness in a grid with seasonal variations as illustrated in section 2.2.1, u is the wind speed at 10 m and u_t is the threshold wind speed, whose exceedance initiates dust emission and depends on the surface characteristics. The most commonly used value for the natural dust emission threshold, that is, wind speed $u_t = 7 \text{ m s}^{-1}$ (Helgren and Prospero, 1987; Chomette et al., 1999; Marsham et al., 2011; Chen et al., 2013, 2014a,b), was employed in our simulations. In addition, soil moisture reinforces inter-particle cohesion forces, reducing the possibility for dust emission (Fécan et al., 1998; Sekiyama and Tanaka, 2011). Therefore, surfaces with high soil moistures and snow cover fractions were excluded from the simulations.

2.2.3. Anthropogenic dust emissions

Anthropogenic dust emissions can be divided into direct and indirect emissions. More specifically, indirect anthropogenic dust emissions are derived from the wind-driven erosion in surfaces modified by human activity; this dust emission mechanism is similar to that of natural dust (Xi and Sokolik, 2016). Thus, the simplified MB scheme was also employed to simulate indirect anthropogenic dust emissions, and the typical parameter of threshold wind velocity for anthropogenic dust emission was utilized. It is notable that the surficial crust is commonly broken by human activity, making soil particles more susceptible to erosion (Li et al., 2017a,b; Xi and Sokolik, 2015; Munkhtsetseg et al., 2017), thereby resulting in a decrease in the threshold wind speed for indirect anthropogenic dust emissions (Gillette and Passi, 1988; Tegen et al., 2004). As noted in Ginoux et al. (2012), the valid range of threshold wind velocity for anthropogenic dust emission was from 6.5 to 13 m s^{-1} , and the smallest value 6.5 m s^{-1} was used in the indirect anthropogenic dust emission simulations, consistent with Xi and Sokolik, 2016. Additionally, bare surfaces with high snow covers and soil moistures were also excluded.

Direct anthropogenic dust emissions are originated from direct human influences and have a strong dependence on the intensity of human endeavors (Guan et al., 2016). The STIRPAT (stochastic impacts by regression on population, P, affluence, A, and technology, T) model was utilized to simulate direct anthropogenic dust emissions in this study, and the population density (P), and economic development were taken as the driving factors for direct anthropogenic dust emissions. The urbanization was estimated via the CNLI, and the economic development was quantified using Engel's coefficient (EC) and GDP growth. The corresponding formula is as follows:

$$G_2 = \begin{cases} 13.25 \times P^{0.12} \times GDP_{growth}^{0.006} \times EC^{1.67}, & 0.0 < CNLI \leq 0.1 \\ 13.33 \times P^{0.05} \times GDP_{growth}^{0.01} \times EC^{1.37}, & 0.1 < CNLI \leq 0.3 \\ 12.79 \times P^{0.08} \times GDP_{growth}^{0.01} \times EC^{1.15}, & 0.3 < CNLI \leq 1.0 \end{cases} \quad (3)$$

As dust emission schemes utilized in this study are too a little simplified, more detailed dust emission scheme introducing in the effects of soil moisture, dust particle size distributions, cohesion among soil particles will be coupled with WRF-Chem model under the constrain of satellite and situ observations to further investigate natural and anthropogenic dust emissions in our future study.

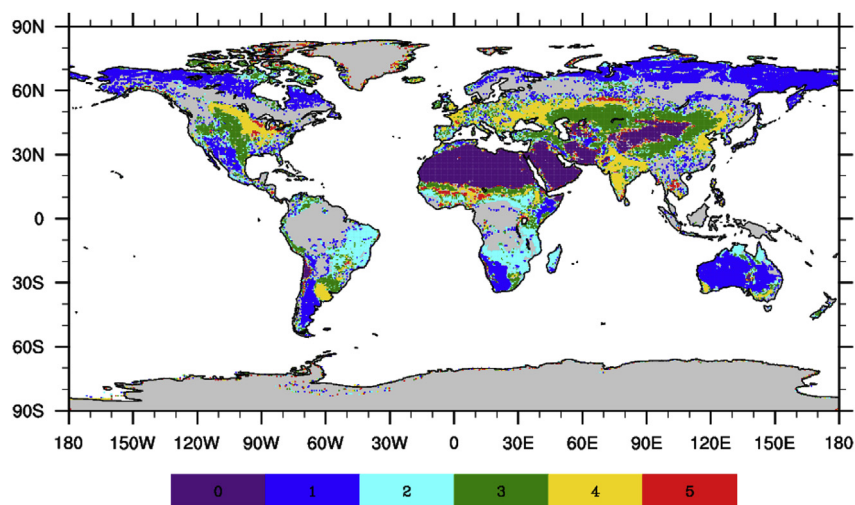


Fig. 1. Land cover types for potential natural and indirect anthropogenic dust sources (see Table 1) from 2007 to 2010.

3. Results

3.1. Dynamic dust source regions

Both natural and anthropogenic land cover types, including desert, gobi desert, open shrub lands, savannas, croplands, grasslands and crop mosaics have the capacities to emit wide distributions of dust particles at the global scale (Fig. 1 and Table 1). Barren or sparsely vegetated areas, open shrub lands, and savannas were selected as the natural land cover types for dust emissions (Table 1). These areas are mainly distributed throughout Australia, northwestern China, West Asia, and the Sahara Desert (Fig. 1). Meanwhile, grasslands, croplands and cropland mosaics were chosen as indirect anthropogenic land cover types (Fig. 1 and Table 1), which is consistent with Huang et al. (2015) and Guan et al. (2016). The anthropogenic dust sources have the characteristics of variable types, dispersion and high spatio-temporal variations due to the variable traffic transportation, cultivation, graze, industrial activities and so on. Therefore, compared with the intensive distributions of potential natural dust sources, the potential anthropogenic dust sources are chiefly located in Central Asia, North America, Europe, the East of China and India. Moreover, they also scatter throughout relatively arid regions, including Australia and South Africa.

The dynamic land cover types for natural and indirect anthropogenic dust emissions identified via the surface bareness were constructed based on the NDVI datasets. The natural dust sources maintains the high value of bare surfaces such as those deserts and gobi desert and their seasonal variations are no more than 1% (Fig. 2c and d) (Tucker et al., 1991; Peters and Eve, 1995; Sobrino and Raissouni, 2000; Bradley and Mustard, 2005; Kim et al., 2013). Moreover, the surface bareness varies in a wide range from 5% to 95% in vegetated surfaces like croplands and grasslands and generally serves as an anthropogenic dust source influenced by human activity. It is obvious that the bareness of potential indirect anthropogenic dust sources is more severe in cold seasons, which exceed 90% of Central Asia and North America. Conversely, it decreases significantly in warm seasons with only

approximately 10% due to vegetation growth. The variations are in good consistent with the previous results provided by Kim et al. (2013) and Chen et al. (2017c) (Fig. 2a and b).

The monthly average natural and indirect anthropogenic surface bareness extents are further compared. The intensity of anthropogenic surface bareness is far less than that of natural surface bareness with differences exceeding 20%. Apparently, the anthropogenic and natural surface bareness extents both increase during cold seasons and peak in November with values of approximately 29.40% and 49.17%, respectively, while they decrease during warm seasons (Fig. 3). It is because vegetated regions recover during warm seasons and wither to become sparse vegetated regions even bare ground during cold seasons together with El Niño-Southern Oscillation effect (Xi and Sokolik, 2015).

The potential anthropogenic dust source regions include potential indirect anthropogenic dust sources (i.e., croplands, grasslands, and cropland mosaics) and urban regions that serve as potential direct anthropogenic dust sources. Although the intensity of surface bareness in natural dust sources are much higher than that in anthropogenic dust sources, the area of potential anthropogenic dust sources is interestingly larger than that of potential natural dust sources with areas of $1.61 \times 10^7 \text{ km}^2$ and $1.33 \times 10^7 \text{ km}^2$ in January and $1.54 \times 10^7 \text{ km}^2$ and $1.31 \times 10^7 \text{ km}^2$ in July (Fig. 4), respectively, suggesting that the potential of anthropogenic dust sources to emit dust particles into atmosphere cannot be ignored at the global scale. Moreover, compared with potential natural dust sources, potential anthropogenic dust source has a significant seasonal variation due to vegetation variations related to cultivation (Xi and Sokolik, 2016) and plant growth (Munkhtsetseg et al., 2017).

3.2. Dust emissions in different climatic regions

To investigate the contributions to dust emissions from different land cover types, the divergences between natural and anthropogenic dust emissions in different climatic regions were further estimated in this study. The AI was introduced to classify different climatic regions at the global scale (Fig. 5). Fig. 6 displays the relationship between direct anthropogenic dust optical depth (DOD) with population density, CNLI, GDP growth and soil moisture in different climatic regions, to investigate the influencing factors on direct anthropogenic dust emissions. It is obvious that the direct anthropogenic DOD increases with the rising of population density, CNLI and GDP growth, indicating their significantly positive relationship. Moreover, with the development of urbanization, land cover type in humid regions have modified greatly, and researches showed that regions with paved road are of lower soil moisture and water and soil conservation capacity, resulting in the

Table 1

Land cover types of potential natural and anthropogenic dust source.

Land Covers	Natural dust sources	Land Covers	Anthropogenic dust sources
0	Barren or sparsely vegetated	3	Grasslands
1	Savannas	4	Croplands
2	Grasslands	5	Crop mosaics

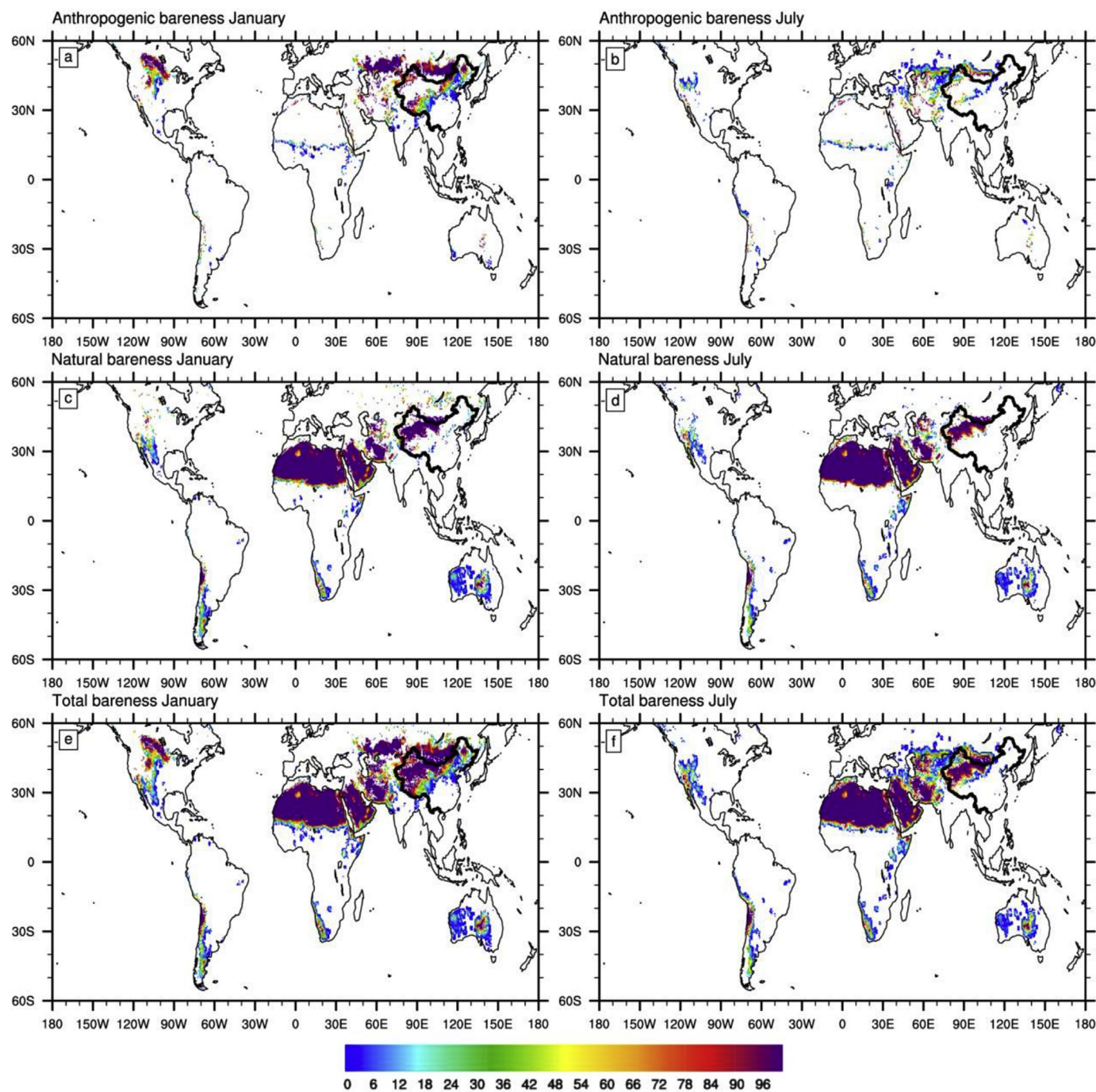


Fig. 2. Anthropogenic (a, b), natural (c, d) and total (e, f) surface bareness (%) in January and July from 2007 to 2010.

higher possibility to emit anthropogenic dust in urban areas (Meiyappan and Jain, 2012). Therefore, the population density, CNLI and GDP growth are employed to simulate the direct anthropogenic dust emissions in this study.

Especially, hyper-arid regions with AI values less than 0.05 are distributed in North Africa, Central Asia and northwestern China, where large deserts such as the Sahara and Taklimakan Deserts are typically located. The GDP growth, population density and urbanization level in hyper-arid regions are quite small (Figure S1). The direct anthropogenic dust optical depth (DOD) in hyper-arid regions was quite small (Fig. 6). Arid and semi-arid regions with AI values ranging from 0.05 to 0.5 are mainly spread throughout West and Central Asia, the North of China, Mongolia, Sahel, Australia, North America and South Africa. The GDP growth, population and urbanization in arid and semi-

arid regions are both higher than those in hyper-arid regions with relatively high value of direct anthropogenic DOD (Fig. 6). This is because that urbanization has been quickening since the 1980s (Chang et al., 2007) and the population density has increased significantly over the past 30 years in semi-arid regions (Guan et al., 2016). Sub-humid and humid regions with AI values of greater than 0.5 are generally distributed throughout East and North Asia, Europe, North America, South America and Middle Africa (Fig. 5). These regions are high-value centers of urbanization, as suggested by their intense human activity and urbanization. It is obvious that the GDP growth, population density and urbanization level in humid regions reach maximum values (Fig. 6), which are considerably higher than those in dryland regions, and thus, humid regions are more likely to emit anthropogenic dust into the atmosphere via human activities and traffic transportation (Zender et al.,

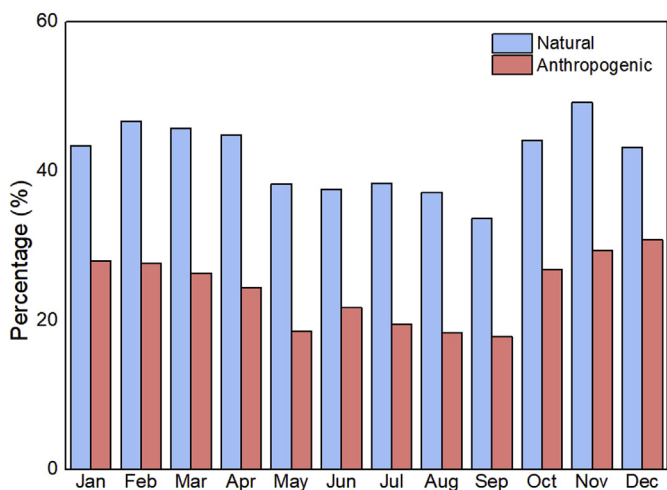


Fig. 3. Global monthly average natural (blue) and anthropogenic (red) bareness (%) within a grid cell from 2007 to 2010.

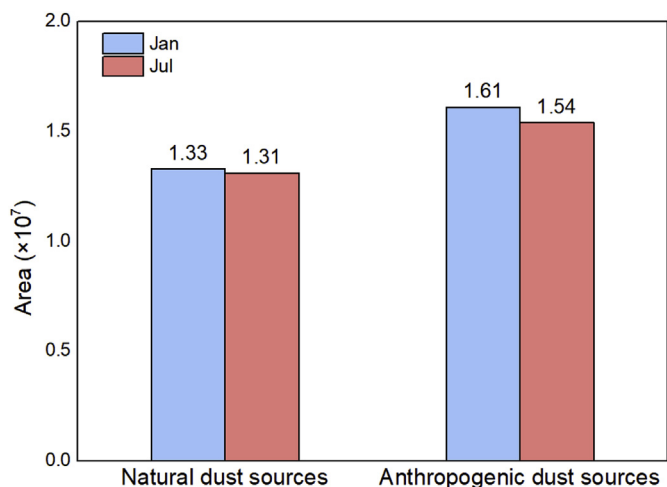


Fig. 4. Total areas (km²) of the natural and the anthropogenic dust sources in January (blue) and July (red) from 2007 to 2010, respectively.

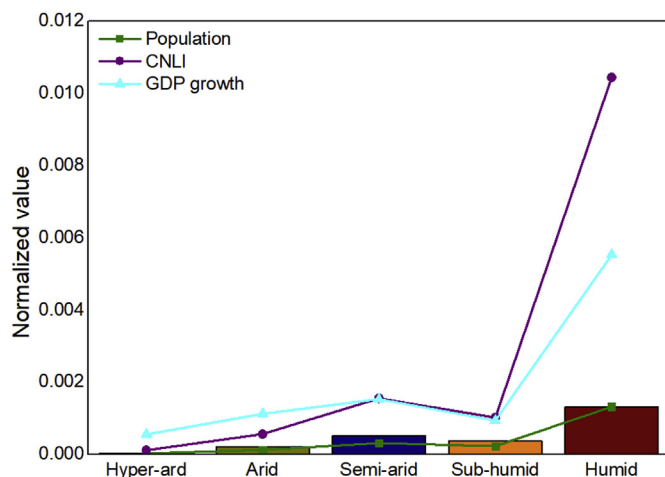


Fig. 6. Normalized mean population density (green line), urbanization level from (purple line), GDP growth (cyan line) and direct anthropogenic dust optical depth (bar chart) from 2007 to 2010 in different climatic regions.

2004; Xi and Sokolik, 2016; Huang et al., 2016a,b, 2017a,b) Therefore, the direct anthropogenic DOD is the largest in humid regions (Fig. 6). It is noted that if the urbanization or economic developments progressed promptly in drylands, the direct anthropogenic emissions would be more severe than those in humid regions at present.

The simulated natural dust emissions primarily derive from large deserts such as Sahara, Taklimakan Desert, deserts in Arabia and Australia, with the annual average natural dust emissions of 12.19 ± 0.24 , 7.31 ± 0.68 , 5.23 ± 0.21 and $0.64 \pm 0.12 \mu\text{g m}^{-2} \text{s}^{-1}$, respectively (Fig. 7). The high value centers and distributions of natural dust emissions are consistent with the WRF-Chem simulations reported by Zhao et al. (2013). In addition, the simulated natural dust emissions also have well agreement with results provided by Chen et al. (2014a) in the Taklimakan Desert (TD), Marsham et al. (2011) and Todd and Guerra, 2016 in Sahara, Kalma et al. (1987) in Australia and Kim et al. (2013) at the global scale. What's more, as the anthropogenic dust is hard to lift up to the planet boundary layer for a long-range transport, the anthropogenic dust column is generally contributed by the anthropogenic dust emissions (Huang et al., 2015). Therefore, to evaluate anthropogenic dust schemes performance in simulating anthropogenic dust emissions, we compared the simulated

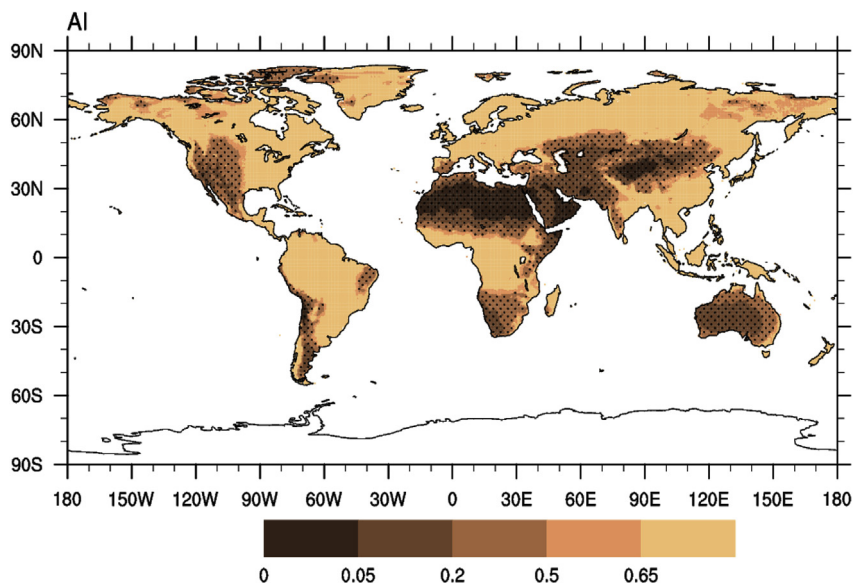


Fig. 5. Spatial distribution of different climatic regions classified by the climatological mean aridity index (AI, unit: dimensionless) from 1948 to 2008.

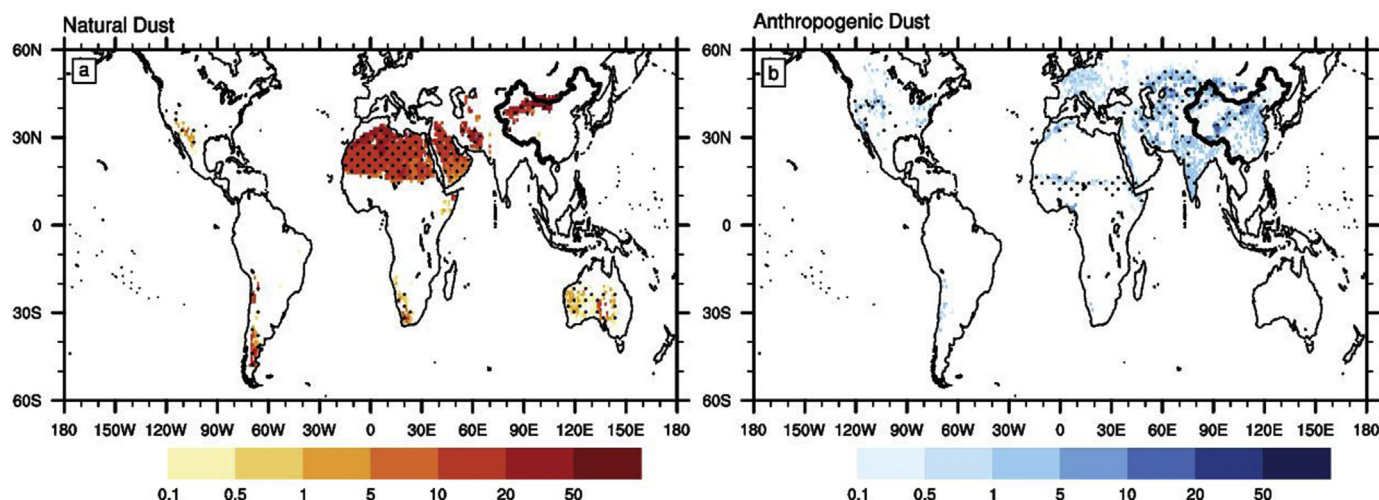


Fig. 7. Spatial distribution of the natural (a) and anthropogenic (b) dust emission fluxes ($\mu\text{g m}^{-2}\text{s}^{-1}$) (shaded areas indicate drylands) from 2007 to 2010.

anthropogenic dust emissions with the CALIPSO anthropogenic dust column from Huang et al. (2015) and Guan et al. (2016). The simulated anthropogenic dust emission fluxes in India, East China, and America are 1.78 ± 0.12 , 1.17 ± 0.08 and $0.08 \pm 0.01 \mu\text{g m}^{-2}\text{s}^{-1}$, respectively, showing great agreement with the distributions of anthropogenic dust column reported by Huang et al. (2015) at the global scale, Wang et al. (2009) in India, Zhang et al. (2016) in the East of China.

Generally, the natural dust sources contributed 81.03% of the global dust emissions and the anthropogenic contributed 18.97% of the residual, similar to those of Ginoux et al. (2012) and Huang et al. (2015) which noted that the anthropogenic dust emissions possesses 25% in total dust emissions. In previous studies, Tegen and Fung (1995) concluded that the fraction of anthropogenic dust emissions is 30–50%. This divergence can be attributed to the detection of anthropogenic dust sources as our results are derived from dynamic dust source function and take the urban areas into consideration.

Further, the spatial distributions of total dust emission fluxes and dust aerosol optical depth (DOD) derived from MISR are displayed in Fig. 8. The high value centers of dust emission flux appeared in the Sahara, the TD, the West of Australia, the East of China and India, having good agreement with the DOD observations including natural dust and anthropogenic dust. Evidently, the simulations results capture the natural dust aerosols in Sahara and west of Australia, and the TD well. For anthropogenic dust emissions, the simulations reproduce the

spatial distributions of anthropogenic dust in the East of China. However, it overestimates the anthropogenic dust aerosols in North America and India because of the uncertainties of direct anthropogenic dust emission scheme (see Fig. 9).

The dust emission fluxes from hyper-arid and arid regions are absolutely predominant, with fluxes reaching $13.12 \mu\text{g m}^{-2}\text{s}^{-1}$ and $4.31 \mu\text{g m}^{-2}\text{s}^{-1}$, respectively. In addition, barren areas contribute 100% and 79.27% to total dust emissions in hyper-arid and arid regions, respectively, indicating natural dust emissions are the major contributor. Moreover, dust emission fluxes were $0.54 \mu\text{g m}^{-2}\text{s}^{-1}$, $0.17 \mu\text{g m}^{-2}\text{s}^{-1}$ and $0.07 \mu\text{g m}^{-2}\text{s}^{-1}$ in semi-arid, sub-humid and humid regions, respectively, which are much smaller than those in hyper-arid and arid regions. In contrast to hyper-arid and arid regions, the main contributors in semi-arid were grasslands, and in sub-humid and humid regions were both urban areas, belonging to the anthropogenic land covers (Fig. 10). The grasslands and urban areas can be classified into the indirect and direct anthropogenic land covers, respectively, contributed 84.72% of total dust emissions in semi-arid regions due to the quick urbanization since 1980s and intense agricultural activity (Chang et al., 2007). The natural land covers including barren areas and open shrub lands contributed the residual 15.19% dust emissions in semi-arid regions. Therefore, in semi-arid and sub-humid regions, both natural and anthropogenic dust emissions are crucial contributors to the overall dust emissions, with anthropogenic dust

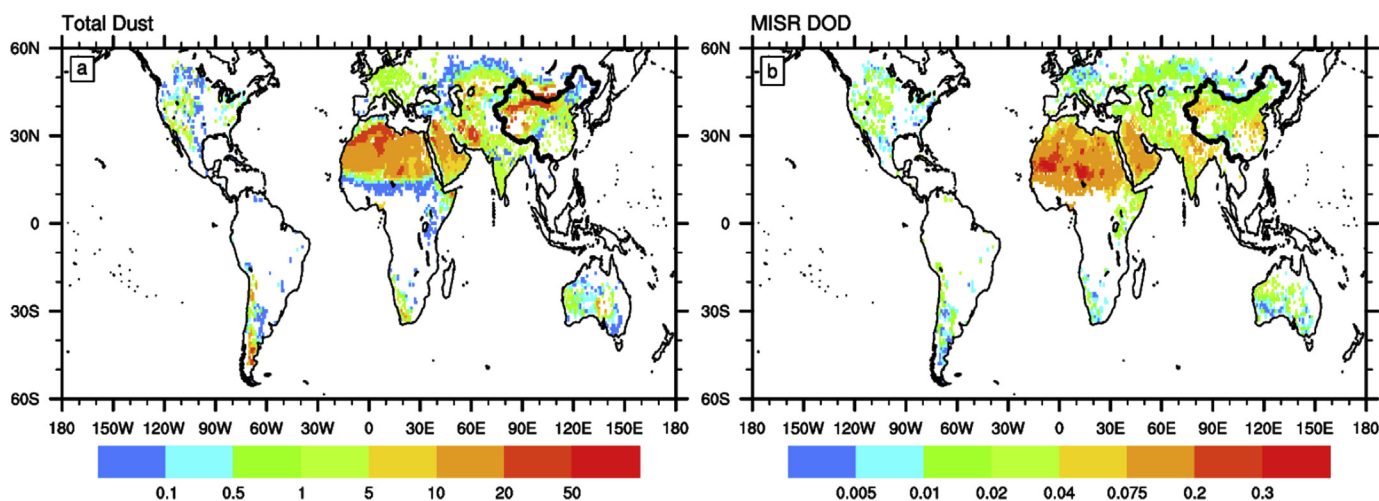


Fig. 8. Spatial distributions of the total dust emission fluxes from 2007 to 2010 ($\mu\text{g m}^{-2}\text{s}^{-1}$) (a) and MISR dust aerosol optical depth (DOD, unit: dimensionless) (b) in 2010.

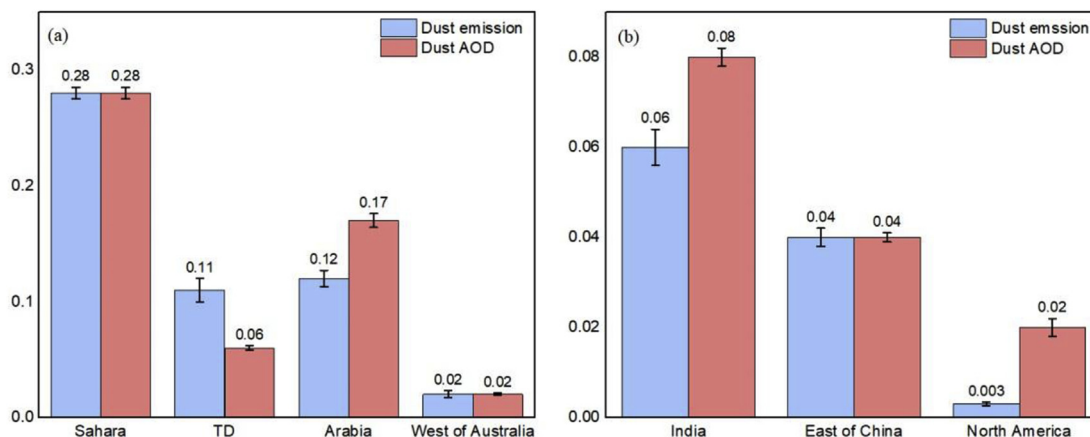


Fig. 9. Normalizations of dust emissions and Dust aerosol optical depth (AOD) derived from MISR in natural (a) and anthropogenic (b) dust sources.

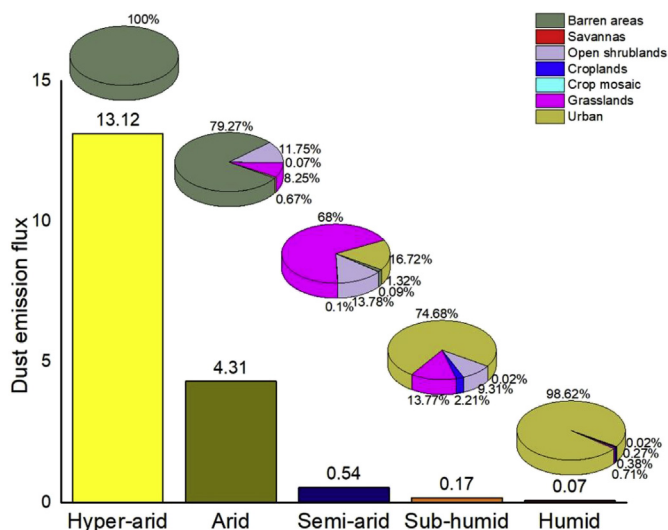


Fig. 10. Contributions (%) of different land cover types to the dust emission flux (pie charts) and the total dust emission flux (columns, $\mu\text{g m}^{-2} \text{s}^{-1}$) in different climatic regions from 2007 to 2010.

emissions superior. Moreover, urban areas prevail over both sub-humid and humid regions with contributions reaching 74.68% and 98.62%, respectively, suggesting that dust emissions with intense human activity must be counted in dust emission simulations. The climatic effects of anthropogenic dust aerosols play an important role in climate changes in semi-arid, sub-humid and humid regions.

Overall, natural dust emissions are mainly derived from hyper-arid and arid regions, and their total contributions can reach up to 99.48%. Furthermore, anthropogenic dust emissions can widely spread across different climatic regions (Fig. 11). It is notable that semi-arid regions are the largest contributors to anthropogenic dust emissions due to comparatively higher emissions from both indirect and direct

anthropogenic dust sources, as they account for 42.99% of the anthropogenic dust emissions at the global scale. It is because that both the population density and urbanization in semi-arid regions ranked only second to those of humid regions. Moreover, compared with humid regions, anthropogenic dust emissions in semi-arid regions were much higher owing to uncomplete constructions of developing regions and smaller soil moisture in semi-arid regions.

4. Discussion and conclusions

Dust is one of the most important components of atmospheric aerosols and consequently plays a crucial part in the hydrologic cycle, the carbon cycle, and the energy budget of the Earth system (Foster and Rideout, 2007; Han et al., 2004, 2010; Chen et al., 2014b; Shao et al., 2011; Hu et al., 2016). To quantitatively estimate the divergences in the natural and anthropogenic dust emission fluxes among different climatic regions, the spatial distributions of both natural and anthropogenic dust emissions from 2007 to 2010 at the global scale were simulated in this study.

Based on the dynamic land cover from NDVI datasets, the results showed that the area of the potential anthropogenic dust sources was $1.61 \times 10^7 \text{ km}^2$ in January and $1.54 \times 10^7 \text{ km}^2$ in July, larger than that of natural dust sources. The natural dust sources were generally sparse vegetation regions, such as deserts, gobi desert, whose surface bareness can reach up to 99% with slight seasonal variations. The global average surface bareness of anthropogenic dust sources was commonly smaller about 20% than that of the natural. In addition, the potential indirect anthropogenic dust sources were vegetation-covered croplands, pasturelands and grasslands, whose bareness changed significantly due to human activity such as cultivation and harvesting with seasonal variations. Therefore, changes in the anthropogenic surface bareness ranged from 5% to 95% in the Central Asia and North America. It is notably that the potential direct anthropogenic dust sources exhibited non-seasonal variations due to the limitations of the available datasets at the global scale.

The simplified natural dust emission scheme proposed by Marsham

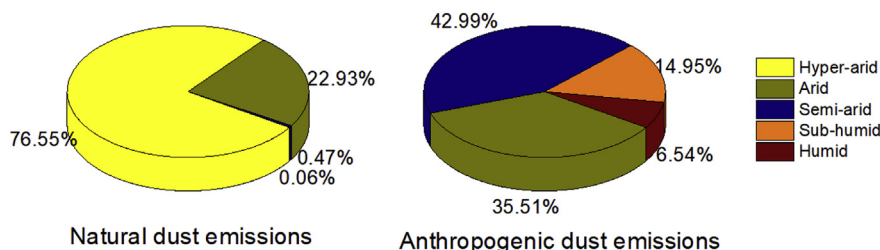


Fig. 11. Contributions of different climatic regions to the natural (left) and the anthropogenic (right) dust emissions from 2007 to 2010.

et al. (2011) and the anthropogenic dust emission schemes constructed based Marsham et al. (2011) were used in this study to simulate the global distributions of natural and anthropogenic dust emissions from 2007 to 2010, respectively. Natural dust emissions were commonly distributed in hyper-arid and arid regions of North Africa, East Asia, and Australia with high-value centers located in the Sahara Desert, the Arabian Peninsula, and the TD. Compared with natural dust emissions, anthropogenic dust emissions exhibited scattered distributions, various sources, small emission magnitudes with high frequencies, and broad spreading in both drylands and humid regions. The high-value centers of anthropogenic dust emissions located in East China, India, North America, Europe and Sahel were related to their population, urbanization and economic development. Natural dust emission fluxes generally ranged from 1 to 50 $\mu\text{g m}^{-2}\text{s}^{-1}$, and anthropogenic dust emission fluxes ranged from 0.1 to 10 $\mu\text{g m}^{-2}\text{s}^{-1}$.

In addition, anthropogenic dust emissions are also widely scattered at the global scale, in contrast to the generally concentrated spatial distributions of natural dust emissions. Notably, anthropogenic dust emissions in developed countries are smaller than those in developing countries. Because incomplete industrial structures, city construction projects, and less restrictive environmental regulations have quite significant impacts on developing countries such as China and India, thereby increasing the possibility potential for the emission of anthropogenic dust particles into the atmosphere over these regions. Accordingly, the environmental policies for emission reduction in developed countries, such as those in Europe and North America, also restrain restricts anthropogenic dust emissions. The natural dust sources contributed 81.32% of the global dust emissions and the anthropogenic contributed the residual 18.68%.

Climatic regions were classified via the AI index into hyper-arid, arid, semi-arid, sub-humid and humid regions. The dust emission fluxes from semi-arid, sub-humid and humid regions were far smaller than those in hyper-arid and arid regions. Generally, natural dust emissions occupied greater proportions in hyper-arid and arid regions, with barren areas accounting for 100% and 79.17% of the total dust emissions in two regions, respectively. Moreover, anthropogenic dust emissions dominated in semi-arid, sub-humid and humid regions, where the major contributors interestingly were grasslands in semi-arid regions and urban areas in sub-humid and humid regions. The grasslands and urban areas contributed 64.01% and 16.98% of the total dust emissions in semi-arid regions, and the urban areas accounted for 75.15% and 98.45% of the total dust emissions in sub-humid and humid regions, respectively, followed by open shrub lands or grasslands. Thus, the impacts of anthropogenic dust aerosols on local climate change in semi-arid, sub-humid and humid regions are necessary.

Notably, dust emissions from semi-arid regions are quite complicated, as they have both natural and anthropogenic dust sources that contribute great amounts of dust emissions, and thus, the climatic effects of dust in semi-arid regions require further investigation. More specifically, the anthropogenic and natural land cover types contributed 80.99% and 19.01% dust emissions in semi-arid region, respectively. Furthermore, it is notable that semi-arid regions were the dominant contributors to the global anthropogenic dust emissions, accounting for 42.99% to the total. The anthropogenic dust emissions from areas with intense direct human activities such as urban in semi-arid regions were higher when compared with that in humid regions. This is because that the humid regions were located in various developed countries whose environmental policies, industrial structures and transportation mechanisms are in complete states, constraining the direct anthropogenic dust emission to a great degree compared with developing countries with various uncomplete constructions in semi-arid regions. What's more, the soil moisture in humid regions was much larger than that in semi-arid regions, which suppress the soil particles uplifting.

Huang et al. (2012, 2016a,b, and 2017a,b) noted that the enhanced warming in drylands under the background of global warming. Recent studies suggested that semi-arid regions contributed 44.46% to the

trend in the annual mean land surface temperature. This temperature increase in cold season over semi-arid regions was 1.5 °C, which was higher than the global annual mean increase over land (1.1 °C) (Huang et al., 2012). Several studies tried to investigate the cause of enhanced warming in drylands from different perspectives, including land-atmosphere interactions, ocean-atmosphere feedback, aerosols, and human activities (He et al., 2014; Huang et al., 2012, 2016a,b; 2017a,b). Huang et al. (2016a,b, 2017a,b) and Guan et al. (2015) noted that the radiation effect of aerosols was an important factor that resulted in enhanced warming in drylands. The latest researches pointed out that the dust could cause warming of the atmosphere through statistical analyses of observational data and global simulations, as dust reduces the outgoing radiation due to its darker appearance over bright surfaces.

The accumulations of anthropogenic dust may significantly heat the atmosphere, strengthen local atmospheric circulation, and modify precipitation efficiency at the local scale, resulting in the inhomogeneous severe warming in semi-arid regions which is the most dominant contributor to anthropogenic dust emissions (Huang et al., 2012). Therefore, complicated anthropogenic and natural dust emission components are capable of being crucial factors in strengthening of warming trends over semi-arid regions. The climate effects of anthropogenic dust especially in urban should be investigated in the future.

Acknowledgments

This research was supported by the Foundation for National Natural Science Foundation of China (No. 41775003), Innovative Research Groups of the National Science Foundation of China (Grant No. 41521004) and the Foundation of Key Laboratory for Semi-Arid Climate Change of the Ministry of Education in Lanzhou University. We would like to thank Center for International Earth Science Information Network (CIESIN), Columbia University, and Centro Internacional de Agricultura Tropical (CIAT) for the population density data used in this study.

Appendix A. Supplementary data

Supplementary data related to this article can be found at <https://doi.org/10.1016/j.atmosenv.2018.07.043>.

References

- Bradley, B.A., Mustard, J.F., 2005. Identifying land cover variability distinct from land cover change: cheatgrass in the Great Basin. *Remote Sens. Environ.* 94, 204–213. <https://doi.org/10.1016/j.rse.2004.08.016>.
- Brown, M.E., Pinzon, J.E., Didan, K., Morisette, J.T., Tucker, C.J., 2006. Evaluation of the consistency of long-term NDVI time series derived from AVHRR, SPOT-Vegetation, SeaWiFS, MODIS and Land-SAT ETM+. *IEEE Trans. Geosci. Rem. Sens.* 44, 1787–1793. <https://doi.org/10.1109/TGRS.2005.860205>.
- Cakmur, R.V., Miller, R.L., Torres, O., 2004. Incorporating the effect of small small journal of Botany, 53(5):379–399. *Geophys. Res. Atmos* 109 (11), 2136–2142. <https://doi.org/10.1029/2003JD004067>.
- Chang, X., Chen, Y., Cui, B., 2007. Urbanization progress influence upon regional desertification process in semi-arid zone. *Arid. Land Geogr.* 30 (3), 321–327 100-6060(2007)03-0321-07 (in Chinese).
- Chomette, O., Legrand, M., Marticorena, B., 1999. Determination of the wind speed threshold for the emission of desert dust using satellite remote sensing in the thermal infrared. *Journal of Geophysical Research Atmospheres* 104 (D24), 31207–31215. <https://doi.org/10.1029/1999jd900756>.
- Chen, S.Y., Huang, J.P., Zhao, C., Qian, Y., Leung, R.L., Yang, B., 2013. Modeling the transport and radiative forcing of Taklimakan dust over Tibetan Plateau: a case study in the summer of 2006. *J. Geophys. Res.* 118, 797–812. <https://doi.org/10.1002/jgrd.50122>.
- Chen, S.Y., Zhao, C., Qian, Y., Leung, R.L., Huang, J.P., Huang, Z.W., Bi, J.R., Zhang, W., Shi, J.S., Yang, L., Li, D.S., Li, J.X., 2014a. Regional modeling of dust mass balance and radiative forcing over East Asia using WRF-Chem. *Aeolian Res.* 15, 15–30. <https://doi.org/10.1016/j.aeolia.2014.02.001>.
- Chen, S.Y., Huang, J.P., Qian, Y., Ge, J.M., Su, J., 2014b. Effects of aerosols on autumn precipitation over Mid-eastern China. *J. Trop. Meteorol.* 20, 242–250. <https://doi.org/10.3969/j.issn.1004-4965.2012.03.006>.
- Chen, S.Y., Huang, J.P., Li, J.X., Jia, R., Jiang, N.X., Kang, L.T., Ma, X.J., Xie, T.T., 2017a.

- Comparison of dust emission, transport, and deposition between the Taklimakan Desert and gobi desert from 2007 to 2011. *Sci. China Earth Sci.* 60, 1–18. [10.1016/j.s11430-016-9051-0](https://doi.org/10.1016/j.s11430-016-9051-0).
- Chen, S.Y., Huang, J.P., Qian, Y., Zhao, C., Kang, L.T., Yang, B., Wang, Y., Liu, Y.Z., Yuan, T.G., Wang, T.H., Ma, X.J., Zhang, G.L., 2017b. An overview of mineral dust modeling over East Asia. *J. Meteor. Res.* 31, 633–653. <https://doi.org/10.1007/s13351-017-6142-2>.
- Chen, S.Y., Huang, J.P., Kang, L.T., Zhang, H., Ma, X.J., He, Y.L., Yuan, T.G., Yang, B., Huang, Z.W., Zhang, G.L., 2017c. Emission, transport and radiative effects of mineral dust from Taklimakan and Gobi Deserts: comparison of measurements and model results. *Atmos. Chem. Phys.* 17, 1–43. <https://doi.org/10.5194/acp-17-2401-2017>.
- Dai, A., 2016. Future warming patterns linked to today's climate variability. *Sci. Rep.* 6, 19110.
- Dee, D.P., Uppala, S.M., Simmons, A.J., Berrisford, P., Poli, P., Kobayashi, S., Andrae, U., Balmaseda, M.A., Balsamo, G., Bauer, P., Bechtold, P., Beljaars, A.C.M., van de Berg, L., Bidlot, J., Bormann, N., Delsol, C., Dragani, R., Fuentes, M., Geer, A.J., Haimberger, L., Healy, S.B., Hersbach, H., Hölm, E.V., Isaksen, I., Kållberg, P., Köhler, M., Matricardi, M., McNally, A.P., Monge-Sanz, B.M., Morcrette, J.J., Park, B.K., Peubey, C., Rosnay, P., de Tavolato, C., Thépaut, J.N., Vitart, F., 2011. The ERA-Interim reanalysis: configuration and performance of the data assimilation system. *Quart. J. Roy. Meteor. Soc.* 137 (656), 553–597. <https://doi.org/10.1002/qj.828>.
- Elvidge, C.D., Baugh, K.E., Kihn, E.A., Kroehl, H.W., Davis, E.R., Davis, C.W., 1997. Relation between satellite observed visible, near infrared emissions, population and energy consumption. *Int. J. Remote Sens.* 18, 1373–1379.
- Evan, A.T., Flamant, C., Gaetani, M., Guichard, F., 2016. The past, present and future of African dust. *Nature* 531, 493–495. <https://doi.org/10.1038/nature17149>.
- Fécan, F., Marticorena, B., Bergametti, G., 1998. Parameterization of the increase of the aeolian erosion threshold wind friction velocity due to soil moisture for arid and semi-arid areas. *Ann. Geophys.* 17 (1), 149–157. <https://doi.org/10.1007/s00585-999-0149-7>. (Source: OAI).
- Feng, S., Fu, Q., 2013. Expansion of global drylands under a warming climate. *Atmos. Chem. Phys.* 13, 10081–10094. <https://doi.org/10.5194/acp-13-10081-2013>.
- Foster, J.C., Rideout, W., 2007. Storm Enhanced Density: Magnetic Conjugacy Effects. *Annales Geophysicae*, vol. 25. pp. 5911–5915. <https://doi.org/10.5194/angeo-25-1791-2007>. (8).
- Friedl, M.A., McIver, D.K., Hodges, J.C.F., Zhang, X.Y., Muchoney, D., Strahler, A.H., Woodcock, C.E., Gopal, S., Schneider, A., Cooper, A., Baccini, A., Gao, F., Schaaf, C., 2002. Global land cover mapping from MODIS: algorithms and early results. *Remote Sens. Environ.* 83, 287–302. [https://doi.org/10.1016/S0034-4257\(02\)00078-0](https://doi.org/10.1016/S0034-4257(02)00078-0).
- Friedl, M.A., Sulla-Menashe, D., Tan, B., Schneider, A., Ramankutty, N., Sibley, A., Huang, X., 2010. MODIS Collection 5 global land cover: algorithm refinements and characterization of new datasets. *Remote Sens. Environ.* 114, 168–182. <https://doi.org/10.1016/j.rse.2009.08.016>.
- Gillette, D.A., Passi, R., 1988. Modeling dust emission caused by wind erosion. *J. Geophys. Res.* 93 (D11), 14,233–14,242. <https://doi.org/10.1029/JD093iD11p14233>.
- Ginoux, P., Chin, M., Tegen, I., Prospero, J.M., Holben, B., Dubovik, O., Lin, S.J., 2001. Sources and distributions of dust aerosols simulated with the GOCART model. *J. Geophys. Res.* 106 (D17), 20255–20273. <https://doi.org/10.1029/2000JD000053>.
- Ginoux, P., Prospero, J.M., Gill, T.E., Christina, N.H., Zhao, M., 2012. Global with the GOCART model. *J. el. J. I. J. le aerosol products. Globalprospero, J. M., Gill, T. E., Christina, N. H., Zhao, M., 2012. Rev. Geophys.* 50 (3), 3005. <https://doi.org/10.1029/2012RG000388>.
- Gong, S.L., Zhang, X.Y., Zhao, T.L., 2003. Characterization of soil dust aerosol in China and its transport and distribution during 2001 ACE-Asia: 2. Model simulation and validation. *J. Geophys. Res.* 108. <https://doi.org/10.1029/2002JD002633>. 4262–4234.
- Gong, S.L., Zhang, X.Y., Zhao, T.L., Barrie, L.A., 2004. Sensitivity of Asian dust storm to natural and anthropogenic factors. *Geophys. Res. Lett.* 31, L07210. <https://doi.org/10.1029/2004GL019502>.
- Gong, S.L., Zhang, X.Y., Zhao, T.L., Zhang, X.B., Barrie, L.A., McKendry, I.G., Zhao, C.S., 2006. A simulated climatology of Asian dust aerosol and its trans-Pacific transport. Part II: interannual variability and climate connections. *J. Clim.* 19, 104–122. <https://doi.org/10.1175/JCLI3606.1>.
- Guan, X., Huang, J., Guo, R., Yu, H., Lin, P., Zhang, Y., 2015. Role of radiatively forced temperature changes in enhanced semi-arid warming in the cold season over East Asia. *Atmos. Chem. Phys.* 15, 13777–13786. <https://doi.org/10.5194/acp-15-13777-2015>.
- Guan, X.D., Huang, J., Zhang, Y., Xie, Y., Liu, J., 2016. The relationship between anthropogenic dust and population over global semi-arid regions. *Atmos. Chem. Phys.* 16, 5159–5169. <https://doi.org/10.5194/acp-16-5159-2016>.
- Han, Z., Ueda, H., Matsuda, K., Zhang, R., Arao, K., Kanai, Y., Hasome, H., 2004. Model study on particle size segregation and deposition during Asian dust events in March 2002. *J. Geophys. Res.* 109, 4321–4339. <https://doi.org/10.1029/2004JD004920>.
- Han, Z., 2010. Direct radiative effect of aerosols over East Asia with a regional coupled climate/chemistry model. *Meteorol. Z.* 19, 287–298. <https://doi.org/10.1127/0941-2948/2010/0461>.
- He, Y., Huang, J., Ji, M., 2014. Impact of land–sea thermal contrast on interdecadal variation in circulation and 496 blocking. *Clim. Dynam.* 43, 3267–3279. <https://doi.org/10.1007/s00382-014-2103-y>.
- Helgren, D.M., Prospero, J.M., 1987. Wind velocities associated with dust deflation events in the Western Sahara. *J. Clim. Appl. Meteorol.* 26, 1147–1151.
- Huang, J., Guan, X., Ji, F., 2012. Enhanced cold-season warming in semi-arid regions. *Atmos. Chem. Phys.* 12, 5391–5398. <https://doi.org/10.5194/acp-12-5391-2012>.
- Huang, J., Ji, M., Xie, Y., Wang, S., He, Y., Ran, J., 2016a. Global semi-arid climate change over last 60 years. *Clim. Dynam.* 46, 1131–1150. <https://doi.org/10.1007/s00382-015-2636-8>.
- Huang, J., Li, Y., Fu, C., Chen, F., Fu, Q., Dai, A., Shinoda, M., Ma, Z., Guo, W., Li, Z., Zhang, L., Liu, Y., Yu, H., He, Y., Xie, Y., Guan, X., Ji, M., Lin, L., Wang, S., Yan, H., Wang, G., 2017a. Dryland climate change recent progress and challenges. *Rev. Geophys.* 55, 719–778. <https://doi.org/10.1002/2016RG000550>.
- Huang, J., Liu, J., Chen, B., Nasiri, S.L., 2015. Detection of anthropogenic dust using CALIPSO lidar measurements. *Atmos. Chem. Phys.* 15, 11653–11665. <https://doi.org/10.5194/acp-15-11653-2015>.
- Huang, J., Yu, H., Dai, A., Wei, Y., Kang, L., 2017b. Drylands face potential threat under 2°C global warming target. *Nat. Clim. Change* 7 (6), 417–422. <https://doi.org/10.1038/NCLIMATE3275>.
- Huang, J., Yu, H., Guan, X., Wang, G., Guo, R., 2016b. Accelerated dryland expansion under climate change. *Nat. Clim. Change* 6, 166–171. <https://doi.org/10.1038/nclimate2837>.
- Hulme, M., 1996. Recent climatic change in the world's drylands. *Geophys. Res. Lett.* 23, 61–64. <https://doi.org/10.1029/95GL03586>.
- Huneus, N., Schulz, M., Balkanski, Y., 2010. Global dust model intercomparison in AeroCom phase I. *Atmos. Chem. Phys.* 10 (10), 7781–7816. <https://doi.org/10.5194/acp-11-7781-2011>.
- Hu, Z., Zhao, C., Huang, J., Leung, L.R., Qian, Y., Yu, H., Huang, L., Kalashnikova, O.V., 2016. Trans-Pacific transport and evolution of aerosols: evaluation of quasi-global WRF-Chem simulation with multiple observations. *Geosci. Model Dev. (GMD)* 9, 1725–1746. <https://doi.org/10.5194/gmd-9-1725-2016>.
- Joussaume, S., 1990. Three-dimensional simulations of the atmospheric cycle of desert dust particles using a general circulation model. *J. Geophys. Res. Atmos* 95 (D2), 1909–1941. <https://doi.org/10.1029/JD095iD02p1909>.
- Kalashnikova, O.V., Kahn, R.A., 2008. Mineral dust plume evolution over the Atlantic from MISR and MODIS aerosol retrievals. *J. Geophys. Res.* 113 (D24S02). <https://doi.org/10.1029/2008JD010083>.
- Kalma, J.D., Speight, J.G., Wasson, R.J., 1987. Potential wind erosion in Australia: a continental perspective. *J. Clim.* 3, 411–428. [10.1175/1527-0940\(1987\)003<0411:1889.00>2.CO;2](https://doi.org/10.1175/1527-0940(1987)003<0411:1889.00>2.CO;2).
- Kahn, R., Banerjee, P., McDonald, D., Diner, D., 1998. Sensitivity of multiangle imaging to aerosol optical depth and a pure size distribution and composition over ocean. *J. Geophys. Res.* 103, 32,195–32,213. <https://doi.org/10.1029/98JD01752>.
- Kahn, R., Banerjee, P., McDonald, D., 2001. The sensitivity of multiangle imaging to natural mixtures of aerosols over ocean. *J. Geophys. Res.* 106, 18,219–18,238. <https://doi.org/10.1029/2000JD900497>.
- Kang, L.T., Huang, J., Chen, S., 2015. Long-term trends of dust events over Tibetan Plateau during 1961–2010. *Atmos. Environ.* 125, 188–198. <https://doi.org/10.1016/j.atmosenv.2015.10.085>.
- Kang, L.T., Chen, S., Huang, J.P., Zhao, S.M., Ma, X.J., Yuan, T.G., Zhang, X.R., Xie, T.T., 2017. The spatial and temporal distribution of absorbing aerosols over East Asia. *Rem. Sens.* 9, 1050. <https://doi.org/10.3390/rs9101050>.
- Kim, D., Chin, M., Bian, H., Tan, Q., Brown, M.E., Zheng, T., You, R., Diehl, T., Ginoux, P., Kucsera, T., 2013. The effect of the dynamic surface bareness on dust source function, emission, and distribution. *J. Geophys. Res.* 118, 1–16. <https://doi.org/10.1029/2012JD017907>. 2013.
- Kim, D., Chin, M., Kemp, Eric, M., Tao, Z., Peters-Lidard, Chista, D., Ginoux, P., 2017. Development of high-resolution dynamic dust source function: a case study with a strong dust storm in a regional model. *Atmos. Environ.* 159, 11–25. <https://doi.org/10.1016/j.atmosenv.2017.03.045>.
- Largeron, Y., Guichard, F., Bouniol, D., Couvreux, F., Kergoat, L., 2015. Can we use surface wind fields from meteorological reanalyses for Sahelian dust emission simulations. *Geophys. Res. Lett.* 42 (7), 2490–2499. <https://doi.org/10.1002/2014GL062938>.
- Li, J., Lv, Q., Zhang, M., Wang, T., Kawamoto, K., Chen, S., Zhang, B., 2017a. Effects of atmospheric dynamics and aerosols on the fraction of supercooled water clouds. *Atmos. Chem. Phys.* 17, 1847–2863. <https://doi.org/10.5194/acp-17-1847-2017>.
- Li, M., Zhang, Q., Kurokawa, J., Woo, J., He, K., Lu, Z., Ohara, T., Song, Y., Streets, D.G., Carmichael, G.R., Cheng, Y., Hong, C., Huo, H., Jiang, X., Kang, S., Liu, F., Su, H., Zheng, B., 2017b. *Atmos. Chem. Phys.* 17, 935–963. <https://doi.org/10.5194/acp-17-935-2017>.
- Liu, C., Zhao, T.L., Yang, X.H., Liu, F., Han, Y.X., Luan, Z.P., He, Q., Mark, R., Yuen, W.K., 2016. Observational study of formation mechanism, vertical structure, and dust emission of dust devils over the Taklimakan Desert, China. *J. Geophys. Res.* 121 (7), 3608–3618. <https://doi.org/10.1002/2015JD024256>.
- Luan, Z.P., Han, Y.X., Zhao, T.L., Liu, F., Liu, C., 2017. Dust opacities inside the dust devil column in the Taklimakan Desert. *Atmos. Meas. Tech.* 10 (1), 273–279. <https://doi.org/10.5194/amt-2016-231>.
- Mahowald, N., Kohfeld, K., Hansson, M., Balkanski, Y., Harrison, S., Prentice, I.C., Michael, S., Rodhe, H., 1999. Dust sources and deposition during the last glacial maximum and current climate: a comparison of model results with paleodata from ice cores and marine sediments. *J. Geophys. Res. Atmos.* 104 (D13). <https://doi.org/10.1029/1999JD900084>. 895–815.
- Mao, R., Ho, C.H., Shao, Y., Gong, Y., Kim, J., 2011. Influence of arctic oscillation on dust activity over Northeast Asia. *Atmos. Environ.* 45 (2), 326–337. <https://doi.org/10.1016/j.atmosenv.2010.10.020>.
- Mao, R., Ho, C.H., Feng, S., Gong, D.Y., Shao, Y.P., 2013. The influence of vegetation variation on northeast Asian dust activity. *Atmos. Sci.* 49 (1), 87–94. <https://doi.org/10.1007/s13143-013-0010-5>.
- Marshall, J.H., Knippertz, P., Dixon, N.S., Parker, D.J., Lister, G.M.S., 2011. The importance of the representation of deep convection for modeled dust-generating winds over West Africa during summer. *Geophys. Res. Lett.* 38, L16803. <https://doi.org/10.1029/2011GL048368>.
- Marticorena, B., Bergametti, G., 1995. Modeling the atmospheric dust cycle: 1. Design of a soil-derived dust emission scheme. *J. Geophys. Res. Atmos.* 100 (D8), 16415–16430.

- <https://doi.org/10.1029/95JD00690>.
- Marticoarena, B., Bergametti, G., Aumont, B., Callot, Y., N'Doumé, C., Legrand, M., 1997. Modeling the atmospheric dust cycle: 2. Simulation of Saharan dust sources. *J. Geophys. Res. Atmos.* 102 (D4), 4387–4404. <https://doi.org/10.1029/96JD02964>.
- Meiyappan, P., Jain, A.K., 2012. Three distinct global estimates of historical land-cover change and land-use conversions for over 200 years. *Front. Earth Sci.* 6 (2), 122–139. <https://doi.org/10.1007/s11707-012-0314-2>.
- Munkhtsetseg, E., Shinoda, M., Ishizuka, M., Mikami, M., Kimura, R., Nikolich, G., 2017. A livestock trampling function for potential emission rate of wind-blown dust in a Mongolian temperate grassland. *Atmos. Chem. Phys.* 1–27. <https://doi.org/10.5194/acp-2017-94>. 2017.
- Murakami, D., Yamagata, Y., 2017. Estimation of Gridded Population and GDP Scenarios with Spatially Explicit Statistical Downscaling. *ArXiv*, 1610.09041.
- Penner, J.E., Charlson, R.J., Hales, J.M., Laulainen, N.S., Leifer, R., Novakov, T., Ogre, J., Radke, L.F., Schwartz, S.E., Travis, L., 1994. Quantifying and minimizing uncertainty of climate forcing by anthropogenic aerosols. *Bull. Am. Meteorol. Soc.* 75 (No. 3), 380–400.
- Perlwitz, J., Tegen, I., Miller, R.L., 2001. Interactive soil dust aerosol model in the GISS GCM: 1. Sensitivity of the soil dust cycle to radiative properties of soil dust aerosols. *J. Geophys. Res. Atmos.* 106 (D16), 18167–18192. <https://doi.org/10.1029/2000JD900668>.
- Peters, A.J., Eve, M.D., 1995. Satellite monitoring of desert plant community response to moisture availability. *Environ. Monit. Assess.* 37, 273–287. <https://doi.org/10.1007/BF00546895>.
- Qian, Y., Fu, C.B., Wang, S., 1999. Mineral dust and climate change 14 (4), 391–394 (in Chinese).
- Sekiyama, T.T., Tanaka, T.Y., 2011. The effects of snow cover and soil moisture on asian dust: II. Emission estimation by lidar data assimilation. *Solanus* 7 (655), 40–43. <https://doi.org/10.2151/sola.7a-011>.
- Shao, Y.P., Dong, C.H., 2006. A review on East Asian dust storm climate, modelling and monitoring. *Global Planet. Change* 52, 1–22. <https://doi.org/10.1016/j.gloplacha.2006.02.011>.
- Shao, Y.P., Zhao, S.X., 2001. Wind erosion and wind-erosion research. *Ann. Arid Zone* 40 (3), 317–336. https://doi.org/10.1007/978-1-4020-8895-7_1.
- Shao, Y.P., 2004. Simplification of a dust emission scheme and comparison with data. *J. Geophys. Res.* 109, D10202. <https://doi.org/10.1029/2003JD004372>.
- Shao, Y., Raupach, M.R., Leys, J.F., 1996. A model for predicting aeolian sand drift and dust entrainment on scales from paddock to region. *Aust. J. Soil Res.* 34, 309–342. <https://doi.org/10.1071/SR960309>.
- Shao, Y.P., Wyrwoll, K.H., Chappell, A., 2011. Dust cycle: an emerging core theme in Earth system science. *Aeolian. Res.* 2, 181–204. <https://doi.org/10.1016/j.aeolia.2011.02.001>.
- Shukla, J., Mintz, Y., 1982. Influence of land-surface evapotranspiration on the Earth's climate. *Science* 215, 1498–1501.
- Sobrino, J.A., Raissouni, N., 2000. Toward remote sensing methods for land cover dynamic monitoring: application to Morocco. *Int. J. Remote Sens.* 21, 353–366. <https://doi.org/10.1080/014311600210876>.
- Sugimoto, N., Uno, I., Nishikawa, M., Shimizu, A., Matsui, I., Dong, X., Chen, Y., Quan, H., 2003. Record heavy Asian dust in Beijing in 2002: observations and model analysis of recent events. *Geo. Res. Lett.* 30 (16), 87–104. <https://doi.org/10.1029/2002GL016349>.
- Tegen, I., Fung, I., 1994. Modeling of mineral dust in the atmosphere: sources, transport, and optical thickness. *J. Geophys. Res.* 99 (D11), 22897–22914. <https://doi.org/10.1029/94JD01928>.
- Tegen, I., Fung, I., 1995. Contribution to the atmospheric mineral aerosol load from land surface modification. *J. Geophys. Res.* 100 (D9), 18707–18726. <https://doi.org/10.1029/95jd02051>.
- Tegen, I., Werner, M., Harrison, S.P., Kohfeld, K.E., 2004. Relative importance of climate and land use in determining present and future global soil dust emission. *Geo. Res. Letters* 31 (5), 325–341. <https://doi.org/10.1029/2004GL021560>.
- Todd, M., Guerra, C., 2016. Dust aerosol emission over the Sahara during summertime from cloud-aerosol lidar with orthogonal polarization (CALIOP) observations. *Atmos. Environ.* 128, 147–157. <https://doi.org/10.1016/j.atmosenv.2015.12.037>.
- Tucker, C.J., Dregne, H.E., Newcomb, W.W., 1991. Expansion and contraction of the Sahara Desert from 1980 to 1990. *Science (Wash. D C)* 253, 299–301. <https://doi.org/10.1126/science.253.5017.299>.
- Wallace, J.M., Johanson, C.M., 2012. Simulated versus observed patterns of warming over the extratropical northern hemisphere continents during the cold season. *Proc. Natl. Acad. Sci. U.S.A.* 109, 14337–14342.
- Wang, C., Kim, D., Ekman, A.M., Barth, M.C., Rasch, P.J., 2009. Impact of anthropogenic aerosols on Indian summer monsoon. *Geophys. Res. Lett.* 36 <https://doi.org/10.1029/2009GL040114>. 2009.
- Wang, J., Xu, X., Henze, D.K., Zeng, J., Ji, Q., Si-Chee, T., Huang, J., 2012. Top-down estimate of dust emissions through integration of MODIS and MISR aerosol retrievals with the GEOS-Chem adjoint model. *Geophys. Res. Lett.* 39 (8), 8802.
- Wang, Z., Ueda, H., Huang, M., 2000. A deflation module for use in modeling longton module for use in modeling longroc. *Natl Acad. Geophys. Res. Atmos.* 105 (D22), 26947–26960. <https://doi.org/10.1029/2000JD900370>.
- Westphal, D.L., Toon, O.B., Carlson, T.N., 1988. A case study of mobilization and transport of Saharan dust. *J. Atmos. Sci.* 45 (15), 2145–2175. [https://doi.org/10.1175/1520-0469\(1988\)045.<2145:ACSOMA>2.0.CO;2](https://doi.org/10.1175/1520-0469(1988)045.<2145:ACSOMA>2.0.CO;2).
- Woodward, S., 2001. Modeling the atmospheric life cycle and radiative impact of mineral dust in the Hadley Centre climate model. *J. Geophys. Res. Atmos.* 106 (D16), 18155–18166. <https://doi.org/10.1029/2000jd900795>.
- Wu, Z., Huang, N., Wallace, J., Smoliak, B., Chen, X., 2011. On the time-varying trend in global-mean surface temperature. *Clim. Dynam.* 37, 759–773.
- Xi, X., Sokolik, I.N., 2015. Seasonal dynamics of threshold friction velocity and dust emission in Central Asia. *J. Geophys. Res. Atmos.* 120 (4), 1536–1564. <https://doi.org/10.1002/2014JD022471>.
- Xi, X., Sokolik, I.N., 2016. Quantifying the anthropogenic dust emission from agricultural land use and desiccation of the Aral Sea in Central Asia. *J. Geophys. Res. Atmos.* 121 (20). <https://doi.org/10.1002/2016JD025556>.
- Zender, C.S., Bian, H., Newman, D., 2003. Mineral dust entrainment and deposition (DEAD) model: description and 1990s dust climatology. *J. Geophys. Res. Atmos.* 108 (D14), 10–1029. <https://doi.org/10.1029/2002JD002775>.
- Zender, C.S., Miller, R., Tegen, I., 2004. Quantifying mineral dust mass budgets: terminology, constraints, and current estimates. *Eos. Trans. AGU* 85 (48), 509–512. <https://doi.org/10.1029/2004EO480002>.
- Zhoa, C., Chen, S., Leung, L.R., Qian, Y., Kok, J.F., Zaveri, R.A., Huang, J., 2013. Uncertainty in modeling dust mass balance and radiative forcing from size parameterization. *Atmos. Chem. Phys.* 13 (21), 10733–10753. <https://doi.org/10.5194/acp-13-10733-2013>.
- Zhao, C., Liu, X., Leung, L.R., Johnson, B., 2010. The spatial distribution of mineral dust and its shortwave radiative forcing over North Africa: modeling sensitivities to dust emissions and aerosol size treatments. *Atmos. Chem. Phys.* 10, 8821–8838. <https://doi.org/10.5194/acp-10-8821-2010>. 2010.
- Zhao, C., Hu, Z., Qian, Y., Ruby Leung, L., Huang, J., Huang, M., Jin, J., Flanner, M.G., Zhang, R., Wang, H., Yan, H., Lu, Z., Streets, D.G., 2014. Simulating black carbon and dust and their radiative forcing in seasonal snow: a case study over North China with field campaign measurements. *Atmos. Chem. Phys.* 14, 11475–11491. <https://doi.org/10.5194/acp-14-11475-2014>.
- Zhao, C.F., Li, Y., Zhang, F., Sun, Y.L., Wang, P.C., 2018. Growth rates of fine aerosol particles at a site near Beijing in June 2013. *Adv. Atmos. Sci.* 35, 209–217. <https://doi.org/10.1007/s00376-017-7069-3>.
- Zhao, C.F., Klein, S.A., Xie, S.C., Liu, X.H., Boyle, J.S., Zhang, Y.Y., 2012. Aerosol first indirect effects on non-precipitating low-level liquid cloud properties as simulated by CAM5 at ARM sites. *Geophys. Res. Lett.* 39. <https://doi.org/10.1029/2012GL051213>.
- Zheng, Y., Zhao, T.L., Che, H.Z., Liu, Y., Han, Y.X., Liu, C., Xiong, J., Liu, J.H., Zhou, Y.K., 2016. A20-year simulated climatology of global dust aerosol deposition. *Sci. Total Environ.* 557, 861–868. <https://doi.org/10.1016/j.scitotenv.2016.03.086>.
- Zhuo, L., Shi, P.J., Chen, J., Ichinose, T., 2003. Application of compounded night light index derived from DMSP/OLS data to urbanization analysis in China in the 1990s. *Acta Geograph. Sin.* 58, 893–902. <https://doi.org/10.11821/xb200306013>. (In Chinese).
- Zhang, J., Christopher, S.A., 2003. Longwave radiative forcing of Saharan dust aerosols estimated from MODIS, MISR, and CERES observations on Terra. *Geophys. Res. Lett.* 30 (23), 343–354.
- Zhang, Q., Schaaf, C., Seto, K.C., 2013. The Vegetation Adjusted NTL Urban Index: a new approach to reduce saturation and increase variation in nighttime luminosity. *Remote Sens. Environ.* 129 (2), 32–41. <https://doi.org/10.1016/j.rse.2012.10.022>.
- Zhang, Q., Pandey, B., Seto, K.C., 2016. A robust method to generate a consistent time series from DMPS/OLS nighttime light data. *IEEE Trans. Geosci. Rem. Sens.* 54 (10), 5821–5831. <https://doi.org/10.1109/TGRS.2016.2572724>.